Polymer Chemistry

ROYAL SOCIETY OF CHEMISTRY

PAPER

View Article Online
View Journal | View Issue

Cite this: *Polym. Chem.*, 2026, **17**, 670

Degradable vinyl copolymers featuring backbone dithiocarbonates by radical copolymerization of a cyclic xanthate

Kyle S. Hepburn and Peter J. Roth *

Radical thiocarbonyl addition-ring-opening (TARO) copolymerization has emerged as a promising method to install weak linkages into vinyl-based polymers. However, the portfolio of available monomers is limited to thionolactones and cyclic thiocarbamates. Herein, a cyclic xanthate featuring an additional in-ring sulfur atom, 4*H*-1,3-benzoxathiin-2-thione (BOT), was prepared by reacting 2-mercaptobenzyl alcohol with thiophosgene, avoiding the commonplace thionation reaction. An AIBN-initiated radical polymerization of BOT resulted in 37% conversion and approx. 75 mol% ring-opened dithiocarbonate repeat units alongside ring-retained dithioorthoester repeat units. A series of *N*,*N*-dimethylacrylamide (DMA)–BOT copolymers was prepared with copolymer BOT contents ranging from 2.5 mol% to 16 mol% with quantitative ring-opening. BOT was found to be less reactive than DMA with estimated reactivity ratios of r_{DMA} = 2.73 and r_{BOT} = 0.04, which led to BOT incorporation throughout the high-yielding copolymerization in the absence of vinyl homopolymerization reported for the use of other thionolactone monomers. The BOT repeat units were easily cleaved through aminolysis and basic hydrolysis. Uniquely, the dithiocarbonate repeat units featured two cleavable C–S bonds, meaning that the degradant was not retained as a fragment end group. Cyclic xanthates are therefore useful for the preparation of easily degradable acrylamide copolymers.

Received 11th August 2025,
Accepted 11th January 2026

DOI: 10.1039/d5py00805k

rsc.li/polymers

Introduction

The recent advent of radical thiocarbonyl addition-ring-opening (TARO) polymerization[1,2] has enabled the preparation of vinyl polymers containing labile thioester linkages that offer opportunities for recycling,[3] biomedicine,[4,5] 3-D printed materials,[6] and degradable networks[7,8] and adhesives.[9] This method involves the radical ring-opening copolymerization of cyclic thiocarbonyl monomers (thionolactones[1,2,10,11] and cyclic thionocarbamates[12] featuring cyclic –ZC(=S)O–) and the formation of backbone thioesters and thiocarbamates (–ZC(=O)S–). Uniquely, these labile linkages can be cleaved selectively[1,13] in the presence of (oxo)esters. Additional advantages of the method are the stability of many thiocarbonyl monomers under ambient conditions and their rapid incorporation during copolymerizations. This method differs from the copolymerization of cyclic RAFT agents (such as trithiocarbonates) with the latter procedure generating backbone thiocarbonyl groups (–C(=S)S–) that remain susceptible toward radical attack and β-scission, which precludes the formation of high molar mass polymers.[14] The first TARO monomer, thionolactone dibenzo[*c*,*e*]oxepin-5(7*H*)-thione (DOT), was reported independently by our group[1] and Gutekunst[2] in 2019 and has been shown to copolymerize with secondary, more-activated monomers including acrylates,[1,2] acrylamides,[13] and styrene.[3,15] Since then, the family of thiocarbonyl monomers has been expanded to include further aromatic thionolactones,[3,16–18] aliphatic thionolactones,[10,11,19–23] and thionocarbamates,[12] see Scheme 1. The electronic effects of substituents[18,24] and the dihedral angle of the aryl–thiocarbonyl segment[17] have been shown to have strong impacts on the copolymerization kinetics and comonomer compatibility.

However, despite the advantages of TARO polymerization over other types of radical ring-opening polymerizations, the current family of monomers has limitations: first, thionolactones are typically prepared through low-yielding thionations of lactone precursors; second, homopolymerization of TARO monomers remains challenging and, depending on the cyclic monomer, requires elevated temperature,[21] is low yielding,[17,22,25] or does not proceed at all,[10,12] precluding the radical preparation of polythioesters with degradability in every repeat unit; and third, all current TARO monomers provide a single cleavable C–S bond in the backbone. This means that the degrading nucleophile (such as hydroxide,

School of Chemistry and Chemical Engineering, University of Surrey, Guildford, Surrey, GU2 7XH, UK. E-mail: p.roth@surrey.ac.uk

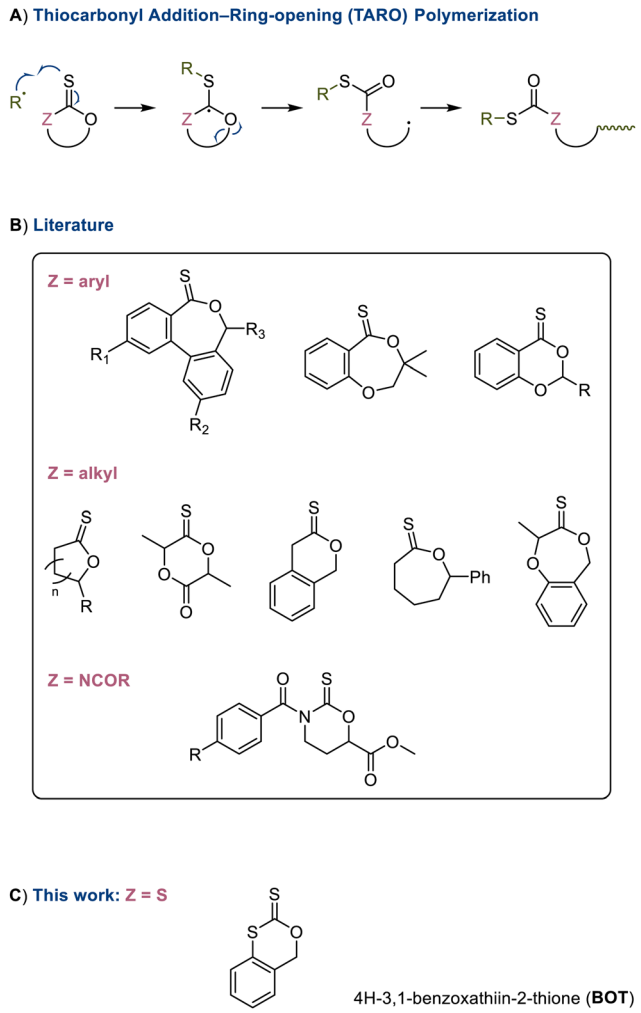

Scheme 1 (A) Mechanism of thiocarbonyl addition-ring-opening (TARO) polymerization to give labile linkages; (B) overview of thionolactone (Z = alkyl/[10,11,19–23]aryl)[1–3,16–18] and *N*-acyl thionocarbamate (Z = NC(═O)R)[12] TARO monomers explored in the literature; and (C) structure of the cyclic xanthate described in this work.

amine, or thiolate) will form the end group of the degraded fragments. The chemical nature of the degradant therefore influences the properties (especially solubility)[13] of the degradation products, making the current portfolio of TARO monomers ill-suited for applications where several degradation mechanisms are possible but where predictable properties of the fragments are required.

Herein, we present the first cyclic xanthate TARO monomer, 4*H*-1,3-benzoxathiin-2-thione (BOT), which was prepared using thiophosgene as a source of the thiocarbonyl motif, thus avoiding a thionation step. While the synthesis was low yielding, it did not require chromatographic separation. During the writing of this manuscript, Gutekunst's group published a cyclic xanthate that underwent topochemical polymerization in bulk following an anionic mechanism.[26] With a conversion of 37%, the AIBN-initiated homopolymerization of BOT was more effective than that of DOT and gave a fully degradable polydithiocarbonate. BOT was found to copolymerize with a selection of secondary, more-activated monomers. (Co) polymerization provided a backbone dithiocarbonate (-SC(═O)S–) functionality. Aminolysis lead to the cleavage of both C–S bonds and full removal of the labile group from the fragments.

Experimental section

Instrumentation

Nuclear magnetic resonance (NMR) spectroscopy was performed using 400 and 500 MHz Bruker instruments in 5 mm NMR tubes. The residual non-deuterated solvent signal of $CDCl_3$ (δ_H = 7.26 ppm) was used as a reference. Melting points were determined using an SMP50 automatic melting point apparatus at a heating rate of 1.0 °C min^{-1}. The melting point was determined by rewatching the video taken by the instrument. Size exclusion chromatography (SEC) analysis was performed using a Viscotek GPC Max VE 2001 GPC. The system was operated at 35 °C with three linear 7.5 mm × 300 mm Phenogel mixed-D columns connected to a refractive index detector. Tetrahydrofuran (THF) was used as the mobile phase at a flow rate of 1 mL min^{-1}. The calibration of the system was based on the molar mass determination of a series of narrow molecular weight distribution poly (methyl methacrylate) (pMMA) standards ranging from 0.88 to 1677 kg mol^{-1}, and the reported values are pMMA-equivalent. Thermogravimetric analysis (TGA) experiments were performed using a TGA Q500 (TA Instruments, New Castle, United States). A sample of 2–5 mg was loaded into a platinum pan and heated at a rate of 10 °C min^{-1} from room temperature to 800 °C under a nitrogen atmosphere at a flow rate of 60 mL min^{-1}. The thermal decomposition temperature was defined as the temperature at which 95% of the original mass remained. Fourier-transform infrared (FT-IR) spectroscopy was performed using a PerkinElmer FT-IR spectrometer under attenuated total reflection (ATR) conditions.

Materials and methods

All reagents were purchased from Sigma-Aldrich and used as received, unless noted otherwise. Ethylamine (2 M in THF) was purchased from Thermo Scientific and diluted with THF (1 : 1 by volume) to give a 1 M solution. Vinyl monomers were deinhibited by passing through a plug of basic alumina to remove inhibitors immediately before polymerization. 2,2′-Azobis(isobutyronitrile) (AIBN) was recrystallized from methanol and stored in a freezer.

Synthesis of 2-mercaptobenzyl alcohol

In analogy to a procedure reported by Roberts and Hartley,[27] thiosalicylic acid (6.32 g, 41 mmol) powder was slowly added to $LiAlH_4$ (2 M in THF, 25 mL, 49 mmol) in an ice bath and under nitrogen. The solution was then stirred at room temperature for 1 h. The solution was cooled in an ice bath and H_2O (8.5 mL) was added dropwise, followed by H_2SO_4 (10%, 40 mL). The solution was allowed to stir under nitrogen for 48 h. The reaction mixture was washed with diethyl ether (2 ×

100 mL) and concentrated *in vacuo* to yield 2-mercaptobenzyl alcohol as an olive-coloured paste (4.8 g, 85% yield).

Synthesis of 4*H*-3,1-benzoxathiin-2-thione (BOT)

Thiophosgene (3.4 mL, 44 mmol) and 2-mercaptobenzyl alcohol (4.4 g, 31 mmol) were added to toluene (anhydrous, 400 mL). Triethylamine (9.1 mL, 62 mmol) dissolved in toluene (anhydrous, 100 mL) was added dropwise at 0 °C under N_2 for 30 min, during which the colour of the reaction mixture changed from red to orange. The mixture was then heated to 80 °C with stirring overnight under N_2, and its colour changed to brown. The reaction mixture was washed with water (400 mL) and the organic phase was concentrated *in vacuo* and then precipitated in hexane and vacuum filtered. The residue was dried *in vacuo* to yield BOT as yellow crystals (0.5 g, 9% yield). ^{1}H NMR (400 MHz, $CDCl_3$) δ/ppm = 7.44 (m, 1 H), 7.39 (m, 2 H), 7.24 (m, 1 H), 5,38 (s, 2H); ^{13}C NMR (126 MHz, $CDCl_3$) δ/ppm = 206.16, 132.19, 130.00, 128.24, 127.80, 126.71, 124.02, 75.23 (supported by the ^{1}H–^{13}C HMBC spectrum); FT-IR ν_{max}/cm^{-1} = 3050 (w, CH), 2900 (w, CH), 2860 (w, CH), 1440 (w, C=C), 1380 (m, C=C), 1180 (m, C=S); needles, m.p. 137–139 °C.

A side product was isolated from the filtrate. After evaporation to dryness, the residual solid was dissolved in a minimal volume of hot ethyl acetate. The solution was cooled gradually, forming crystals, which were separated by vacuum filtration to yield 1-oxa-1′,3,3′-trithia-2,2′-spirobi(1,2,3,4-tetrahydronaphthalene) as a beige powder. ^{1}H NMR (400 MHz, $CDCl_3$) δ/ppm = 7.33–7.07 (m, 8H), 5.11, 4.87 (2 d, J = 14.5 Hz, 2H), 4.02, 3.94 (2 d, J = 14.1 Hz, 2H); ^{13}C NMR (126 MHz, $CDCl_3$) δ/ppm = 136.28, 134.48, 132.12, 130.10, 127.92, 126.35, 125.82, 125.51, 97.60, 65.91, 34.94 (supported by the ^{1}H–^{13}C HMBC spectrum); Ft-IR ν_{max}/cm^{-1} = 3050 (w, CH), 2900 (w, CH), 1015 (m, C–O), 750 (m, C–S); m.p. 149–151 °C.

General procedure for free radical polymerization

BOT and the vinyl comonomer (in varying molar ratios as described in the main text, with total comonomers at 50 or 100 equiv.), AIBN (1 equiv.), and anhydrous toluene were added to a round-bottom flask. The mixture was sealed with a rubber septum and degassed with nitrogen for 30 min through a needle, with a shorter needle fitted for gas release. The tube was heated in an oil bath at 80 or 90 °C for the durations described in the main text. After cooling and exposure to air, the monomer conversion was determined by ^{1}H NMR spectroscopy of a sample of the crude mixture diluted with $CDCl_3$. Polymers were purified by precipitation into a 40-fold excess of methanol or diethyl ether–hexane in a ratio of 1 : 1, followed by centrifugation, decanting, and drying *in vacuo*.

General procedure for RAFT polymerization

The procedure followed the same steps as described above with the difference that *S*-benzyl-*S*′-propyl trithiocarbonate[28] (1 equiv.) was added as the RAFT agent and less AIBN (0.25 equiv.) was used.

Copolymer degradation through aminolysis

The (co)polymer (1–5 mg) was dissolved in ethylamine (1 M in THF, 2 mL) and stirred overnight at RT. The solvent and excess amine were evaporated by blowing in a stream of nitrogen before re-dissolving the dry residue in either THF for SEC analysis or in $CDCl_3$ for NMR analysis.

Copolymer degradation using aqueous NaOH

The copolymer (20 mg) was dissolved in aqueous NaOH solution (3.6 M, 20 mL) and stirred overnight at RT. The mixture was extracted with DCM (2 × 10 mL) and the organic layer was dried and evaporated by blowing in a stream of nitrogen before re-dissolving the dry residue in THF for SEC analysis.

Results and discussion

The purpose of this study was to investigate the (co)polymerization behaviour of the novel cyclic xanthate monomer, BOT. The synthesis of TARO monomers typically involves the thionation of lactones using Lawesson's reagent[1,2] or P_4S_{10}.[10,11] The synthesis of BOT (Scheme 2) instead involved thiophosgene to directly install the essential C=S moiety. However, despite optimization attempts of the reaction conditions, side products were formed, giving a low final yield (9%). Gratifyingly, however, pure BOT could be isolated by precipitation in hexane without the need for column chromatography. Analysis of BOT by ^{1}H (Fig. S1), ^{13}C (Fig. S2), and ^{1}H–^{13}C HMBC (Fig. S3) NMR spectroscopy indicated successful synthesis. In addition to six aromatic carbons, the spectra showed the methylene group as a singlet with δ_H = 5.38 ppm and δ_C = 75.2 ppm and a carbon resonance at δ_C = 206 ppm, characteristic of a xanthate group. FT-IR analysis (Fig. S4) was in agreement, showing a thiocarbonyl resonance at 1180 cm^{-1}. A major side product was isolated and presumed to be 1-oxa-1′,3,3′-trithia-2,2′-spirobi(1,2,3,4-tetrahydronaphthalene) (Scheme 2) based on NMR (Fig. S5–S7) and FT-IR (Fig. S8) analyses and was presumably formed through the combination of two BOT molecules with the elimination of carbonyl sulfide.

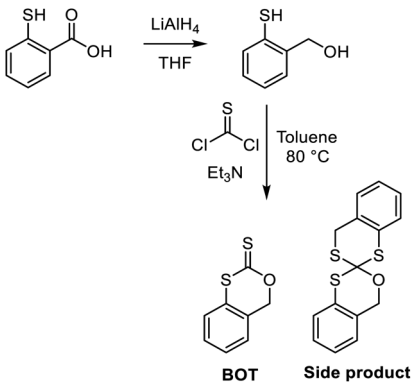

Scheme 2 Synthesis of 4*H*-3,1-benzoxathiin-2-thione (BOT) in a two-step process, with the side product.

The AIBN-initiated homopolymerization of BOT (Scheme 3A) showed a moderate conversion of up to 37%, giving a homopolymer with SEC-measured M_n = 3.2 kg mol^{-1} and $Đ$ = 1.52 (Table 1, entry 1 and Fig. S9). While far from quantitative, this homopolymerization was significantly more efficient than that of DOT, which typically gives 2–13% conversion.[29] The BOT homopolymer was soluble in toluene, DCM, THF, and chloroform and insoluble in hexane, diethyl ether, and water.

The ^{1}H NMR spectrum of pBOT (Table 1, entry 1) is shown in Fig. 1. It showed an aromatic region at δ_H = 7.83–7.10 ppm and an unexpectedly rich aliphatic region at δ_H = 5.31–3.74 ppm with an integral ratio of 4 : 2, suggesting that all aliphatic protons originated from benzylic methylene groups, which was supported by the aliphatic signals being identified as CH_2 groups in a multiplicity-edited (DEPT-135) ^{1}H–^{13}C

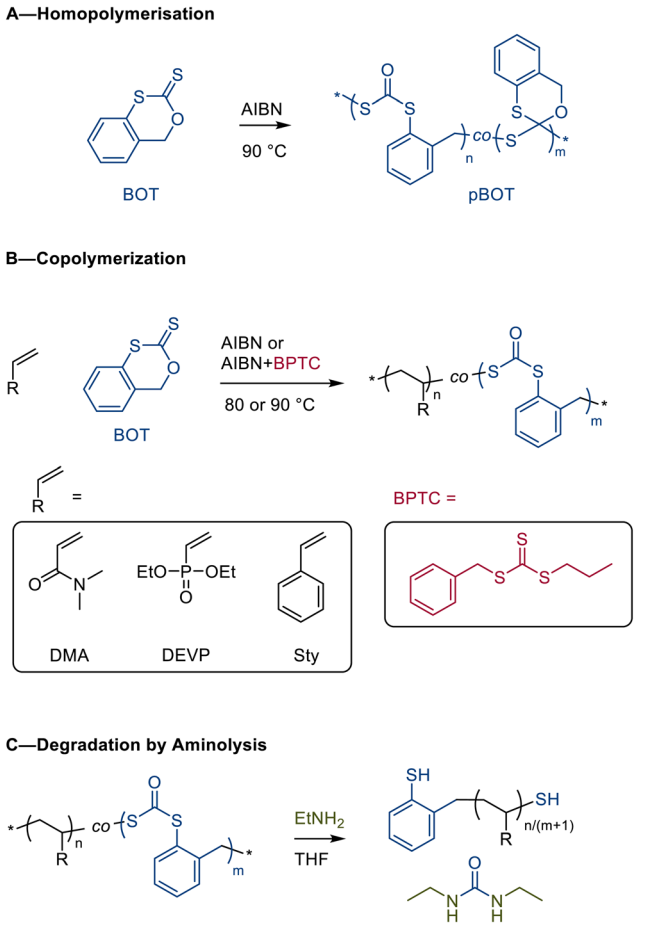

Scheme 3 (A) Homopolymerization of BOT showing ring-opened (~75%) and ring-retained repeat units; (B) BOT copolymerization with vinyl comonomers; and (C) degradation of copolymers by aminolysis.

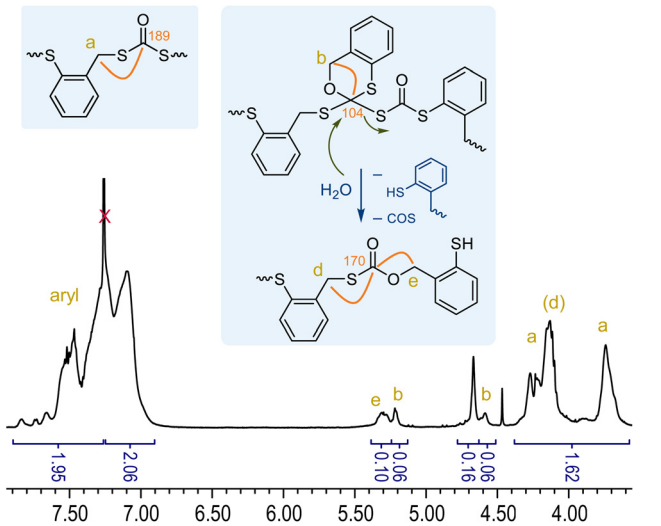

Fig. 1 ^{1}H NMR spectrum of pBOT (Table 1, entry 1) with assignments. The orange numbers refer to the measured ^{13}C chemical shifts (in ppm) found to couple with the assigned protons (orange lines). The proton signal for 'd' is overlapped by the 'a' signal. The green arrows indicate the presumed mechanism for orthocarbonate hydrolysis, showing the degradability of the side product repeat units.

Table 1 List of BOT (co)polymers prepared by TARO (co)polymerization

Entry	Code	Feed (eq.)	Method [a]	Time (h)	Temperature (°C)	Conversion [b] (%)	BOT content [c] (mol%)	Intact M_n^{SEC} (kg mol^{-1})	Intact $Đ$	Degraded [c] M_n^{SEC} (kg mol^{-1})	Degraded [c] $Đ$
1	pBOT	50	FRP	21	90	37	100	3.2	1.52	n.d.	n.d.
2	p(DMA$_{0.97}$-BOT$_{0.03}$)$_n$	97.5 + 2.5	FRP	24	80	99, 100	2.5	0.6	1.44	0.5	1.39
3	p(DMA$_{0.95}$-BOT$_{0.05}$)$_n$	95 + 5	FRP	24	80	100, 99	5	1.6	1.68	1.3	1.07
4	p(DMA$_{0.93}$-BOT$_{0.07}$)$_n$	90 + 10	FRP	24	80	99, 66	7	n.d.	n.d.	n.d.	n.d.
5	p(DMA$_{0.89}$-BOT$_{0.11}$)$_n$	40 + 10	FRP	20	90	100, 52	11	2.0	1.71	0.2	1.91
6	p(DMA$_{0.84}$-BOT$_{0.16}$)$_n$	70 + 30	FRP	15	80	97, 44	16	4.3	1.86	1.1	1.14
7	p(DMA$_{70}$-BOT$_6$)^d	90 + 10	RAFT	5	80	78, 56	7	1.2	1.20	n.d.	n.d.
8	p(DEVP$_{0.4}$-BOT$_{0.6}$)$_n$	33 + 67	FRP	24	90	90, 70	60	4.1	1.75	0.2	2.29
9	p(Sty$_{0.98}$-BOT$_{0.02}$)$_n$	90 + 10	FRP	21	80	51, 7	2	25.3	1.21	6.6	1.73

[a] FRP = free radical polymerization and RAFT agent: *S*-benzyl-*S*′-propyl trithiocarbonate. [b] Estimated from ^{1}H NMR analysis of the polymerization mixture before purification. [c] Aminolysis using ethylamine (1 M in THF). [d] Average number of repeat units for RAFT-made copolymers from comonomer conversions.

HSQC measurement (Fig. S10). The largest peaks in the aliphatic region, labelled 'a' in Fig. 1, were assigned to the methylene group of a ring-opened repeat unit preceding a dithiocarbonate linkage, based on (i) the ^{1}H–^{13}C HSQC spectrum showing an associated carbon shift of δ_C = 35 ppm, characteristic of Ar–*C*H$_2$S– groups and (ii) the ^{1}H–^{13}C HMBC spectrum (Fig. S11) showing coupling to a carbon at δ_C = 189 ppm, characteristic of a dithiocarbonate group. These data confirmed the expected TARO mechanism (Scheme 1A) with ring-opening driven by the formation of a C=O double bond and a stabilised benzylic radical. Additionally, however, signals associated with ring-retained repeat units included a carbon resonance at δ_C = 104 ppm, attributed to an *S*,*S*,*S*,*O*-orthocarbonate, and proton signals at δ_H = 4.59 and 5.22 ppm. Ring retention copolymerization has been documented for aliphatic thionolactones.[30–32] A third set of peaks featured proton signals at δ_H = 5.30 ppm (typical of an Ar–C*H*$_2$O– group) coupling to a carbon signal at δ_C = 170 ppm, typical of monothiocarbonates. These signals were presumed to be associated with orthocarbonate hydrolysis (the mechanism indicated by green arrows in Fig. 1), leading to chain cleavage and a carbonyl moiety in the terminal repeat unit. As the polymerization was conducted in anhydrous toluene, the hydrolysis was presumed to have occurred post-polymerization. Integration of the proton signals indicated a ring-opening efficiency of approx. 75%. Thermogravimetric analysis (TGA) of the homopolymer indicated an initial loss of mass around 100 °C and a maximum decomposition temperature of 258 °C (with an onset of 194 °C) (Fig. S12). Notably, this decomposition temperature was considerably lower than that of DOT (co)polymers, which are typically stable until 330 °C.[8] These data, as well as the accidental hydrolysis of side product repeat groups, demonstrated the enhanced degradability of BOT-based polymers compared to DOT-derived thioesters.

Copolymerization

The AIBN-initiated copolymerization of BOT was investigated using three vinyl comonomers, *N*,*N*-dimethylacrylamide (DMA), diethyl vinylphosphonate (DEVP), and styrene (Sty), with the structures shown in Scheme 3B. Molar BOT feed ratios (using anhydrous toluene as the solvent) ranged from 2.5 to 67 mol%, Table 1, entries 2–10. The conversions of each comonomer pair were determined by ^{1}H NMR analysis before purification based on the disappearance of monomer signals. Copolymerizations of the low (≤5 mol%) BOT feed with DMA showed near-quantitative conversions of both monomers. With a higher feed of BOT, however, its conversion decreased, reducing to 44 mol% conversion at a DMA–BOT feed of 70 : 30, with the DMA conversion remaining near-quantitative (Table 1, entries 2–6). Despite the lower conversions of BOT, it was possible to prepare DMA-based water-soluble copolymers with molar BOT contents ranging from 2.5 to 16%. The SEC curves of the series were monomodal with low measured dispersities in the order of $1.44 \leq Đ \leq 1.86$, in the range expected for a free radical polymerization in the absence of side reactions. A RAFT polymerization mediated by *S*-benzyl-*S*′-propyl-trithiocarbonate of a 90 : 10 DMA–BOT feed gave high conversions of 83% and 56% for DMA and BOT, respectively, and a low SEC-measured dispersity of $Đ$ = 1.20 (Table 1, entry 7), suggesting compatibility of the RAFT process with the TARO polymerization of BOT. Given a previous study demonstrating the production of DOT-rich copolymers from copolymerization formulations containing DEVP, a DEVP–BOT copolymerization with a feed ratio of 33 : 67 was polymerized, resulting in conversions of 90% and 70% for DEVP and BOT, respectively, and a product containing 60 mol% BOT in the absence of any observed ring-retention (*vide infra*) (Table 1, entry 8). A copolymerization with styrene was trialled with a 90 : 10 styrene–BOT feed ratio and gave low conversions of 51% and 7% for styrene and BOT, respectively, suggesting poor compatibility of BOT with styrene (Table 1, entry 9). In some free radical copolymerizations, up to 10 mol% side product was formed and, based on NMR analysis, found to be identical to the spiro by-product formed during BOT synthesis. Conversely, during the RAFT copolymerization of DMA and BOT, nearly 40 mol% of the BOT feed was converted into the spiro side product, suggesting the participation of the RAFT agent in its formation. The side product was fully removed during precipitation of the copolymers, leading to pure products.

The ^{1}H NMR spectrum of p(DMA$_{0.89}$-BOT$_{0.11}$)$_n$ (Table 1, entry 5), as a representative example, is shown in Fig. 2. In addition to the broad aromatic signals at δ_H = 7.47–7.10 ppm (attributed to the BOT repeat units), the spectrum showed several peaks between δ_H = 5.12 and 4.16 ppm. The most prominent of these, a broad singlet at δ_H = 4.54 ppm, was identified as a CH/CH$_3$ group (see the ^{1}H–^{13}C HSQC spectrum in Fig. S13) and found to couple to the amide carbon (δ_C = 174 ppm) of the DMA repeat units and a carbon signal at δ_C = 188 ppm, attributed to dithiocarbonate linkages derived from the ring-opening BOT repeat units, and assigned to the DMA methine preceding a dithiocarbonate, confirming copolymerization and ring-opening, see Fig. S14 and S15. Signals of a

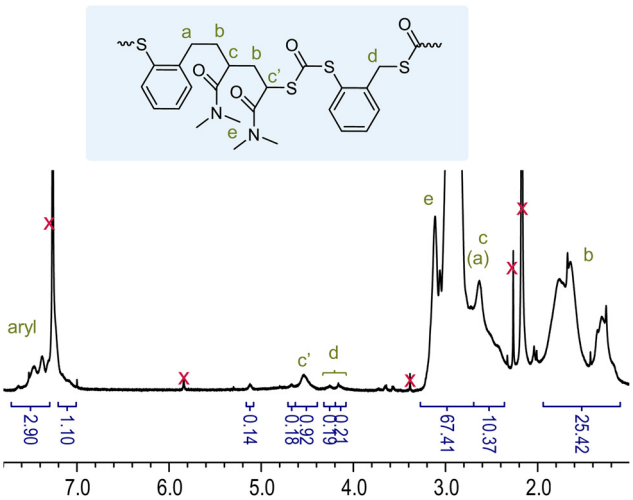

Fig. 2 ^{1}H NMR spectrum of p(DMA$_{0.89}$-BOT$_{0.11}$)$_n$ (Table 1, entry 5).

CH_2 group at δ_H = 4.26 and 4.16 ppm were attributed to the methylene group within a BOT–BOT diad, supported by coupling to the BOT aromatics, see Fig. S15. Weak resonances at δ_H = 5.12 and 4.68 ppm remained unattributed as no coupling in the 2-D spectra could be observed. A comparison with the ^{1}H NMR spectrum of the pBOT homopolymer (Fig. 1) suggested that these signals could stem from ring-retained BOT repeat units. Integration of the ^{1}H NMR spectrum of p($DMA_{0.89}$-$BOT_{0.11}$)$_n$ (and considering whether signals were associated with CH_2 or CH groups) indicated that over 70% of (ring-opened) BOT repeat units were preceded by a DMA repeat unit, demonstrating the successful incorporation of degradable linkages into the DMA backbone.

The free radical copolymerization kinetics were investigated with a 90 : 10 DMA–BOT feed (Table 1, entry 5), see Fig. 3. DMA was found to convert faster than BOT, reaching near-quantitative conversion after 3 hours. The incorporation of BOT was somewhat slower and began to plateau after 1 hour, approaching 65% conversion. The spiro side product was formed at an approximately constant rate during the reaction, consuming 12% of the BOT monomer by the end of the experiment. The kinetics data showed that both monomers were consumed simultaneously, resulting in copolymer chains containing BOT units throughout the reaction. Reactivity ratios were estimated by non-linear least-squares fitting of the conversion data with a numerical solution of the Mayo–Lewis equation to be r_{DMA} = 2.73 and r_{BOT} = 0.04, demonstrating the faster incorporation of DMA but nonetheless leading to the incorporation of BOT, see Fig. S16.

Additionally, we explored the RAFT copolymerization kinetics using the same 90 : 10 DMA–BOT feed ratio and a trithiocarbonate RAFT agent (Scheme 3B and Table 1 entry 7). After a short (30 min) induction period, the conversions of both comonomers increased, reaching a plateau of 78% for DMA and 56% for BOT after 2 h, see Fig. 4. Similar to the FRP experiment, both comonomers were consumed simultaneously, with a faster incorporation of DMA. Under RAFT conditions, this results in copolymers with minimal gradient within the copolymer chains. Surprisingly, however, significantly more side products (mainly the spiro compound discussed above) were formed, reaching 35% after 2 h, suggesting the involvement of RAFT end groups in their formation.

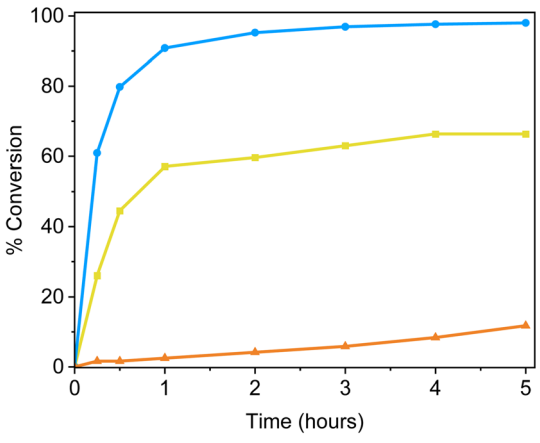

Fig. 3 Free radical copolymerization kinetics of p($DMA_{0.93}$-$BOT_{0.07}$)$_n$ (Table 1, entry 4): DMA (blue circles), estimated BOT incorporation (yellow squares), and side-product formation from the BOT monomer (orange triangles, estimated from the observed loss of BOT).

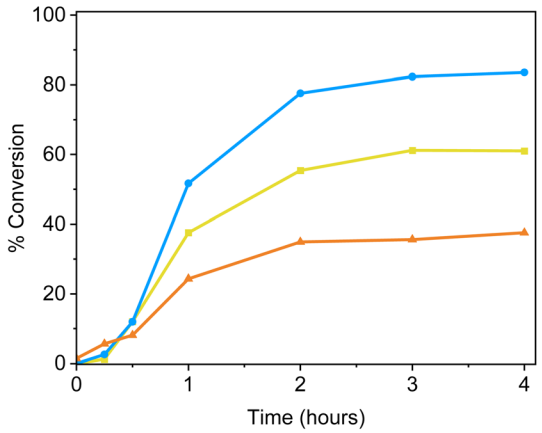

Fig. 4 RAFT kinetics of p(DMA_{70}-BOT_6) (Table 1, entry 7): DMA (blue circles), estimated BOT incorporation (yellow squares), and side-product formation from the BOT monomer (orange triangles, estimated from the observed loss of BOT).

Of note, the prototypical TARO monomer DOT was shown to have higher reactivity than DMA, which typically leads to the full consumption of DOT within the first hours of copolymerization, followed by homopolymerization of (up to 30%) the residual DMA feed and the formation of non-degradable sections.[13] While BOT suffers from the formation of (removable) side-products, its lower reactivity leads to incorporation throughout the polymerization, albeit with the cumulative BOT content lower than the feed (see Table 1). The lower reactivity of BOT compared to DOT is presumed to originate from the electron donation of the additional in-ring sulfur atom to the thiocarbonyl group, which reduces its double bond character.[14]

The copolymerization of BOT with DEVP led to a BOT-rich species, p($DEVP_{0.4}$-$BOT_{0.6}$) with SEC-measured M_n = 4.1 kg mol^{-1} and $Đ$ = 1.75 (Table 1, entry 8). Its ^{1}H NMR spectrum showed a 3 : 2 molar composition (within the integration error of the overlapping signals), see Fig. 5. Its ^{13}C NMR spectrum contained a resonance at δ_C = 188 ppm, indicating the successful ring-opening of BOT and the formation of dithiocarbonate moieties. A signal at δ_H = 3.82 ppm (labelled 'c' in Fig. 5) was assigned to DEVP methine groups preceding a dithiocarbonate linkage based on (i) the ^{1}H–^{13}C HSQC spectrum (Fig. S17) identifying the signal as CH or CH_3; (ii) ^{1}H–^{31}P ^{1}J coupling being evident from a comparison of the ^{1}H and ^{1}H $\{^{31}P\}$ spectra (Fig. S18); and (iii) the ^{1}H–^{13}C HMBC spectrum (Fig. S19) showing coupling to the DEVP backbone methylene and the BOT dithiocarbonate groups, confirming a linkage between the two comonomers. The assignment of the residual signals was supported by a ^{1}H–^{1}H COSY NMR spectrum

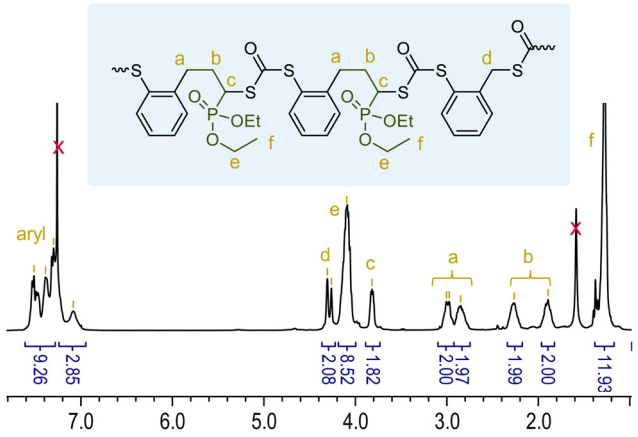

Fig. 5 ^{1}H NMR spectrum of p(DEVP$_{0.4}$-BOT$_{0.6}$)$_n$ (Table 1, entry 8).

(Fig. S20). Despite the high BOT content, the DEVP copolymer showed no sign of ring-retaining polymerization of BOT.

The copolymerization of BOT with styrene in a 90 : 10 feed ratio resulted in low conversions (51% for Sty and 7% for BOT) and isolation of the copolymer p(Sty$_{0.98}$-BOT$_{0.02}$)$_n$ containing 2 mol% of BOT (Table 1, entry 9). Interestingly, SEC analysis showed a relatively high M_n = 25.3 kg mol^{-1} with a narrow dispersity of $Đ$ = 1.21, suggesting the occurrence of radical storage through reversible deactivation,[22,33] presumably based on the reversible addition of BOT to the styrene-based radical chain end forming an *S*,*S*,*S*,*O*-orthocarbonate, as demonstrated for the case of thionoisochromanone.[22] ^{1}H NMR spectroscopy (Fig. 6) showed an unidentified CH/CH$_3$ signal at δ_H = 2.90 ppm, coupling through one bond to a signal at δ_C = 35.8 ppm (Fig. S21) and, through multibond correlation, to a signal at δ_C = 174.9 ppm (Fig. S22). The absence of coupling to aromatic signals and the upfield shift compared to other –C*H*SC(=O)R moieties observed herein and in the literature suggested that this signal did not originate from a styrene methine group. Additional work, beyond the scope of the current study, is required to elucidate the full copolymerization behaviour of BOT with styrene. However, the ^{1}H NMR spectrum showed evidence of successful, albeit little, ring-opening inclusion of BOT through weak signals between δ_H = 3.90 and 4.60 ppm, leading to degradable backbone units, as discussed below. The BOT-derived environment labelled 'a' is similar to the styrene-derived environment labelled 'c', resulting in overlapping signals.

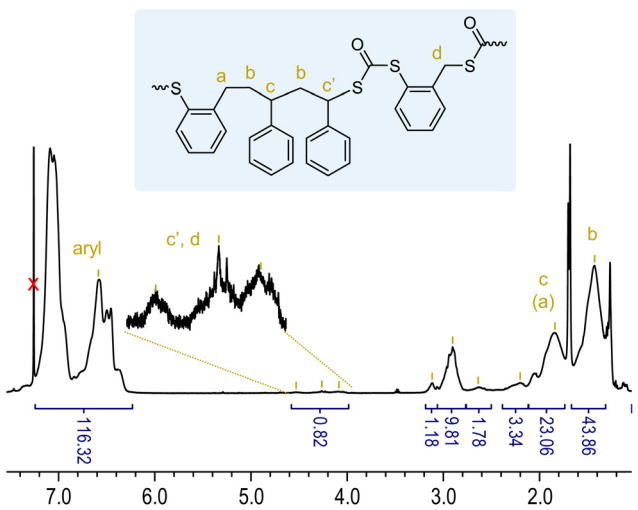

Fig. 6 ^{1}H NMR spectrum of p(Sty$_{0.98}$-BOT$_{0.02}$)$_n$ (Table 1, entry 9).

Degradation

With a series of BOT homo- and copolymers in hand, we next explored the degradation of the in-chain dithiocarbonate linkages through aminolysis and basic hydrolysis. Two DMA

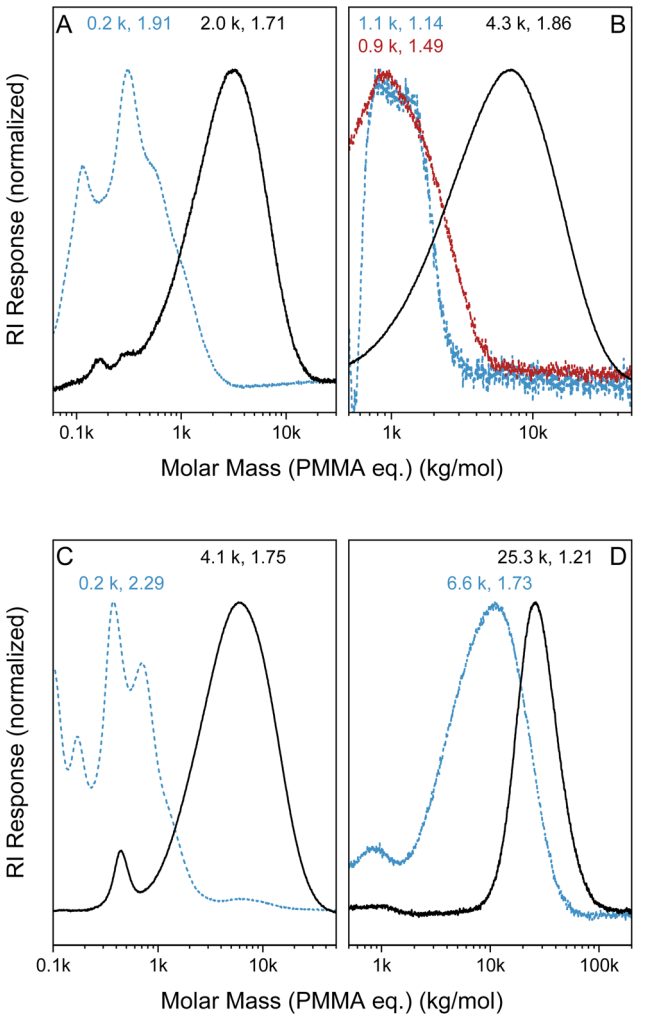

Fig. 7 SEC curves of intact polymers (black lines) and after degradation with ethylamine (1 M in THF, dashed blue lines) or NaOH (3.6 M in water, the dashed red line) for (A) p(DMA$_{0.89}$-BOT$_{0.11}$)$_n$ (Table 1 entry 5); (B) p(DMA$_{0.84}$-BOT$_{0.16}$)$_n$ (entry 6); (C) p(DEVP$_{0.4}$-BOT$_{0.6}$)$_n$ (entry 8); and (D) p(Sty$_{0.98}$-BOT$_{0.02}$)$_n$ (entry 9). The numbers indicate the estimated molar mass and dispersity, respectively. The estimated molar masses of the degraded fragments for (A) and (C) are imprecise as they are outside of the calibration range and appear to overlap with solvent signals.

copolymers, $p(DMA_{0.89}\text{-}BOT_{0.11})_n$ (Table 1 entry 5) and $p(DMA_{0.84}\text{-}BOT_{0.16})_n$ (Table 1 entry 6), were dissolved in ethylamine (1 M in THF) at RT overnight. After evaporation of volatiles, the residual polymers were analysed by SEC and found to have a significantly decreased molecular weight compared to the intact samples before degradation, see Fig. 7A and B. Notably, the complete disappearance of the intact copolymer distribution indicated that even in these copolymers made by free radical polymerization, all chains contained degradable dithiocarbonates, in agreement with the kinetics discussed above. Taking advantage of its water solubility, degradation of $p(DMA_{0.84}\text{-}BOT_{0.16})_n$ was also performed using aqueous NaOH and gave a similar SEC-measured curve as for aminolysis, suggesting complete cleavage of the backbone thioesters, see Fig. 7B. The largest shift in the SEC-measured molecular weight upon degradation was found for the aminolysis of $p(DEVP_{0.4}\text{-}BOT_{0.6})_n$, in agreement with the large BOT content and the expected formation of small molar mass degradation products, see Fig. 7C. Conversely, the aminolysis of the styrene copolymer, $p(Sty_{0.98}\text{-}BOT_{0.02})_n$, resulted in a modest shift from 25.3 kg mol^{-1} to 6.6 kg mol^{-1}, in agreement with a lower content of degradable dithiocarbonates in the backbone. As such, the degradation chemistry—aminolysis and hydrolysis—of the BOT copolymer was found to be similar to that known for the thioester analogues produced from conventional DOT. However, treatment of the BOT homopolymer with ethylamine resulted in the formation of *N*,*N*′-diethylurea (as confirmed by ^{1}H and ^{13}C NMR spectroscopy, Fig. S23 and S24), confirming the cleavage of both C–S bonds of the dithiocarbonate linkages and removal of the carbonyl group from the backbone. The degradant thus is not retained as a fragment end group. Surprisingly, the ^{1}H NMR spectrum of the aminolysed pBOT sample retained some broad aromatic signals, suggesting incomplete degradation of the homopolymer. A ^{13}C NMR signal at δ_C = 173.3 ppm was presumed to stem from the monothiocarbonate end groups that were not aminolysed, showing different reactivities of the backbone linkages obtained from BOT homopolymerization.

Conclusion

The thionation-free synthesis of a novel TARO monomer, BOT, proceeded in a low overall yield but without the need for chromatographic separation. The presence of an additional in-ring sulfur atom (compared to aliphatic and aromatic thionolactones) reduced the radical reactivity of BOT but, somewhat counterintuitively, led to the incorporation of degradable dithiocarbonate units throughout the polymerization (as illustrated by a numerical solution of the Mayo–Lewis equation) without the formation of homovinyl groups found in DOT copolymerization after the complete consumption of DOT. While ring-retention copolymerization was observed especially during the radical homopolymerization of BOT, the resulting dithioorthoester repeat units were easily cleavable. It is anticipated that insights obtained in this study can guide the future development of scalable TARO monomers with ideal copolymerization behaviour.

Conflicts of interest

There are no conflicts to declare.

Data availability

The data supporting this article have been included as part of the supplementary information (SI). Supplementary information: 1-D and 2-D NMR spectra and FT-IR spectra of BOT, the spiro side product, and BOT copolymers; SEC and TGA of the BOT homopolymer, estimation of reactivity ratios, and NMR spectra after degradation. See DOI: https://doi.org/10.1039/d5py00805k.

References

1 N. M. Bingham and P. J. Roth, *Chem. Commun.*, 2019, **55**, 55–58.
2 R. A. Smith, G. Fu, O. McAteer, M. Xu and W. R. Gutekunst, *J. Am. Chem. Soc.*, 2019, **141**, 1446–1451.
3 G. R. Kiel, D. J. Lundberg, E. Prince, K. E. L. Husted, A. M. Johnson, V. Lensch, S. Li, P. Shieh and J. A. Johnson, *J. Am. Chem. Soc.*, 2022, **144**, 12979–12988.
4 N. M. Bingham, Q. un Nisa, P. Gupta, N. P. Young, E. Velliou and P. J. Roth, *Biomacromolecules*, 2022, **23**, 2031–2039.
5 M. Lages, T. Pesenti, C. Zhu, D. Le, J. Mougin, Y. Guillaneuf and J. Nicolas, *Chem. Sci.*, 2023, **14**, 3311–3325.
6 N. Gil, C. Thomas, R. Mhanna, J. Mauriello, R. Maury, B. Leuschel, J. P. Malval, J. L. Clement, D. Gigmes, C. Lefay, O. Soppera and Y. Guillaneuf, *Angew. Chem., Int. Ed.*, 2022, **61**, e202117700.
7 F. Dawson, T. Kazmi, P. J. Roth and M. Kopeć, *Polym. Chem.*, 2023, **14**, 5166–5177.
8 H. Elliss, F. Dawson, Q. U. Nisa, N. M. Bingham, P. J. Roth and M. Kopeć, *Macromolecules*, 2022, **55**, 6695–6702.
9 R. Abu Bakar, K. S. Hepburn, J. L. Keddie and P. J. Roth, *Angew. Chem., Int. Ed.*, 2023, **62**, e202307009.
10 O. Ivanchenko, U. Authesserre, G. Coste, S. Mazières, M. Destarac and S. Harrisson, *Polym. Chem.*, 2021, **12**, 1931–1938.
11 C. M. Plummer, N. Gil, P.-E. Dufils, D. J. Wilson, C. Lefay, D. Gigmes and Y. Guillaneuf, *ACS Appl. Polym. Mater.*, 2021, **3**, 3264–3271.
12 A. Calderon-Diaz, A. C. Boggiano, W. Xiong, N. Kaiser and W. R. Gutekunst, *ACS Macro Lett.*, 2024, **13**, 1390–1395.
13 N. M. Bingham, Q. U. Nisa, S. H. L. Chua, L. Fontugne, M. P. Spick and P. J. Roth, *ACS Appl. Polym. Mater.*, 2020, **2**, 3440–3449.

14 N. M. Bingham, Z. Abousalman-Rezvani, K. Collins and P. J. Roth, *Polym. Chem.*, 2022, **13**, 2880–2901.
15 N. Gil, B. Caron, D. Siri, J. Roche, S. Hadiouch, D. Khedaioui, S. Ranque, C. Cassagne, D. Montarnal, D. Gigmes, C. Lefay and Y. Guillaneuf, *Macromolecules*, 2022, **55**, 6680–6694.
16 P.-E. Dufils, C. M. Plummer, D. J. Wilson, D. Gigmes and Y. Guillaneuf, Thionolactones, Processes of synthesis, uses as comonomers and for polymer functionalization and degradation, WO2023006580, 2023.
17 M. F. I. Rix, K. Collins, S. J. Higgs, E. M. Dodd, S. J. Coles, N. M. Bingham and P. J. Roth, *Macromolecules*, 2023, **56**, 9787–9795.
18 K. Ko, D. J. Lundberg, A. M. Johnson and J. A. Johnson, *J. Am. Chem. Soc.*, 2024, **146**, 9142–9154.
19 O. Ivanchenko, S. Mazières, S. Harrisson and M. Destarac, *Polym. Chem.*, 2022, **13**, 5525–5529.
20 R. Kamiki, T. Kubo and K. Satoh, *Macromol. Rapid Commun.*, 2023, **44**, e2200537.
21 B. Luzel, N. Gil, P. Desiree, J. Monot, D. Bourissou, D. Siri, D. Gigmes, B. Martin-Vaca, C. Lefay and Y. Guillaneuf, *J. Am. Chem. Soc.*, 2023, **145**, 27437–27449.
22 E. A. Prebihalo, A. M. Luke, Y. Reddi, C. J. LaSalle, V. M. Shah, C. J. Cramer and T. M. Reineke, *Chem. Sci.*, 2023, **14**, 5689–5698.
23 Y. Xiong, Z.-B. Lu, Y.-Z. Zhao, L. Xia, C.-Y. Hong, Z. Zhang and Y.-Z. You, *Polym. Sci. Technol.*, 2025, **1**, 468–475.
24 B. Luzel, L. Raggio, E. Benharrous, J. Monot, D. Bourissou, D. Siri, D. Gigmes, C. Lefay, B. Martin-Vaca and Y. Guillaneuf, *Macromolecules*, 2025, **58**, 4627–4635.
25 M. P. Spick, N. M. Bingham, Y. Li, J. De Jesus, C. Costa, M. J. Bailey and P. J. Roth, *Macromolecules*, 2020, **53**, 539–547.
26 A. Calderón-Díaz, L. Ordner, M. G. Bernbeck, M. Palesati, M. Weber, N. Stingelin and W. R. Gutekunst, *J. Am. Chem. Soc.*, 2025, **147**, 21331–21338.
27 C. F. Roberts and R. C. Hartley, *J. Org. Chem.*, 2004, **69**, 6145–6148.
28 J. Y. Quek, P. J. Roth, R. A. Evans, T. P. Davis and A. B. Lowe, *J. Polym. Sci., Part A: Polym. Chem.*, 2013, **51**, 394–404.
29 T. Kazmi, K. S. Hepburn, Q. Nisa, S. Neogi, N. M. Bingham and P. J. Roth, *Macromolecules*, 2025, **58**, 9617–9628.
30 O. Ivanchenko, S. Mazières, S. Harrisson and M. Destarac, *Macromolecules*, 2023, **56**, 4163–4171.
31 O. Ivanchenko, S. Mazières, S. Mallet-Ladeira, S. Harrisson and M. Destarac, *Macromolecules*, 2024, **57**, 8059–8066.
32 O. Ivanchenko, S. Mazières, R. Poli, S. Harrisson and M. Destarac, *Polym. Chem.*, 2022, **13**, 6284–6292.
33 A. A. Toy, H. Chaffey-Millar, T. P. Davis, M. H. Stenzel, E. I. Izgorodina, M. L. Coote and C. Barner-Kowollik, *Chem. Commun.*, 2006, 835–837, DOI: 10.1039/B515561D.